JOURNAL OF Applied Polymer SCIENCE

Investigation on β-Polypropylene/PP-g-MAH/Surface Treated Talc Composites

Jiawei Duan, Qiang Dou*
College of Materials Science and Engineering, Nanjing University of Technology, Nanjing 210009, China
Correspondence to: Q. Dou (E-mail: douqiang.njut@163.com)

ABSTRACT: β-Polypropylene composites containing talc treated by titanate coupling agent (T-talc) and maleic anhydride grafted PP (PP-*g*-MAH) were prepared by melt compounding. The crystallization, morphology, and mechanical properties of the composites were investigated by means of differential scanning calorimetry (DSC), wide angle X-ray diffraction (WAXD), polarized light microscopy (PLM), scanning electron microscopy (SEM), and mechanical tests. It is found that β nucleating agent (NT-C) induces the formation of β-phase but T-talc suppresses the formation of β-modification. Both NT-C and T-talc greatly decrease the spherulitic size of PP. PP-*g*-MAH has a weak restraint on the formation of β-form PP but it improves the compatibility between T-talc and PP matrix. Izod notched impact strength of β-PP/T-talc composite is higher than that of PP/T-talc composite at each loading, indicating the toughening effect of β-PP. Incorporation of PP-*g*-MAH into β-PP/T-talc composite further increases the impact strength when T-talc concentration is below 2.5 wt %. The non-isothermal crystallization kinetics of β-PP composites is well described by Jeziorny's and Mo's methods, respectively. The activation energies (ΔE) of non-isothermal crystallization were calculated by Kissinger method. It is found that NT-C and T-talc accelerate the crystallization rate of PP but PP-*g*-MAH has a slightly negative influence on the crystallization rate of β-PP. © 2013 Wiley Periodicals, Inc. J. Appl. Polym. Sci. 130: 206–221, 2013

KEYWORDS: composites; crystallization; polyolefins; structure–property relations; mechanical properties

Received 30 November 2012; accepted 14 February 2013; published online 8 March 2013
DOI: 10.1002/app.39178

INTRODUCTION

Incorporation of inorganic fillers into plastics is a cheap method to modify the properties of the base materials. Many kinds of fillers such as talc,[1,2] $CaCO_3$,[3] and mica[4] were added to polypropylene (PP) with the purpose of reducing the production cost and improving the stiffness and strength. Talc was among the first fillers used in PP. Numerous literatures reported the mechanical properties, melting, and crystallization behaviors, rheological properties, dispersion characteristics, melt flow rates, and coupling mechanism of PP/talc composites.[1,5–9] Talc is a kind of mineral material with high surface energy and inherently poor interaction with non-polar PP with low surface tension. Therefore, various surface treatments such as maleic anhydride grafted PP (PP-*g*-MA)[1] and titanate coupling agents[9,10] had been used in PP/talc composites.

Isotactic PP (iPP) is a polymorphic material with three known crystal forms, namely α, β, and γ forms. Among them, the β form of iPP has attracted many researchers' interests because of its unique properties, such as improved toughness and formation of microvoids from the β–α transformation, which had been used as toughened plastics products, microporous membrane, microporous fibers, etc. β-iPP can be obtained by β-nucleating agents,[11–13] isothermal crystallization,[14] the temperature slope method,[15] shear,[16] other polymers[17] and fillers.[18,19] Among them, the introduction of β-nucleating agents is the most effective method for the formation of β-phase iPP.

In recent years, some researchers investigated the inorganic particulates-filled β-PP composites. It was found that some surface treated fillers could induce the formation of β-PP. Zhang et al.[20] reported $CaCO_3$ treated by nonionic modifier (polyoxyethylene nonyphenol) induced the formation of β-form PP, and Izod notched impact energy of the composites was significantly increased. Meng and Dou[3,21] used pimelic acid (PA) as a new surface modifier for wollastonite and $CaCO_3$, the β phase contents were enhanced by calcium pimelate formed by the treatments, and the toughness of the composites was improved obviously. Dou et al.[4] found that mica (MC) treated by PA induced a large amount of β-iPP and increased the notched impact strength of iPP/MC composites dramatically. Li and Dou[22,23] used malonic acid (MA) to treat nano-$CaCO_3$ and wollastonite, the β phase contents and toughness of iPP composites were improved by the treatment. Zhang et al.[18,19] also found

nano-$CaCO_3$ supported by PA was a highly efficient β-nucleating agent for PP. Some researchers added inorganic fillers into β-PP matrix. Han et al.[24] added a β-phase nucleating agent (TMB-5) into iPP/$CaCO_3$ composites and found that annealing was beneficial to the improvement of toughness and stiffness and largely enhanced heat distortion temperature. Mai et al.[25] reported that β-nucleating agent and nano-$CaCO_3$ had heterogeneous nucleation and synergistic effects on β-nucleation of ethylene–propylene random copolymer (PPR). Prachum et al.[26] studied the physical and mechanical properties of PP/PP-*g*-MAH/organo-montmorillonite nanocomposites modified with the aryl amide β-nucleator. It was found that β-nucleation increased the tensile elongation at break and crystallization temperature but did not further increase the impact property of nanocomposites. Zhang et al.[27] investigated the crystallization behaviors of iPP containing multi-walled carbon nanotubes (MWCNTs) and a rare earth β-nucleator (WBG). It was found that MWCNTs were active filler to induce α-nucleation but WBG served as β-nucleating agent. Lin et al.[28] found that eggshell (ES) modified by PA was a β nucleating agent with high efficiency and selectivity. ES slightly decreased tensile and flexural properties of PP, but it increased the impact strength of PP. Varga and Toth[29] studied the crystallization and mechanical property of β-PP/talc composites and found that talc was a strong selective α-nucleating agent and suppressed the formation of β-modification. The elastic modulus and yield stress improved but tensile strength decreased with the increasing content of talc. Tjong and Li[6] studied the mechanical behavior of injection-molded talc filled β-iPP composites. Talc exhibited beneficial reinforcing effect in composites, but suppressed the formation of β-form dramatically. The toughness decreased significantly when talc content was above 5 wt %. Fujiyama[30] added γ-quinacridone (GQ, β-crystal nucleator) to iPP filled with talc, mica, and glass flake, respectively. The β-crystal contents were reduced by the filling of particulates. Particulates deteriorated the enhanced impact strength of β-iPP.

In this study, β-PP was prepared by using a commercial β nucleating agent (NT-C), and β-PP composites containing titanate treated talc and PP-*g*-MAH were also prepared. We want to study the influence of a selective α-nucleating agent (talc) and a compatibilizer (PP-*g*-MAH) on the crystallization, morphology, and mechanical properties of β-phase PP.

EXPERIMENTAL

Materials

PP pellets (EPF30R, ~4% ethylene content, MFR = 11 g/10 min at 230°C and 2.16 Kg) were produced by PetroChina Dushanzi Petrochemical (Dushanzi, China). Talc with an average size of 5 μm, was supplied by Haicheng Jinghua Mineral Products (Haicheng, China). PP-*g*-MAH (MAH grafting ratio = 0.3 wt %, MFR = 50 g/10 min at 230°C and 2.16 Kg) was obtained from Qiangren Plastics (Nanjing, China). The industrial antioxidant B215 (Nanjing Hua Lim, Nanjing, China), titanate coupling agent [NDZ201, isopropyl tri(dioctylpyrophosphate) titanate;Nanjing Shuguang Chemical, Nanjing, China], petroleum ether (Wuxi Yasheng Chemical, Wuxi, China) were commercially available. β nucleating agent (NT-C, carboxylate, its FTIR spectrum and application are shown in literatures[31–33]) were obtained from Nanjing Chengkuan Trade (Nanjing, China). All were used as received.

Surface Treatment of Talc

Talc was adequately dried in an oven at 120°C for 4 h. About 500 g talc was added into a high speed blender. And, a solution of 5 g titanate coupling agent in 10 g petroleum ether was put into the blender. The mixture was stirred at 25,000 rpm for 5 min. Then the mixture was dried to constant weight at 100°C. The treated talc was labeled as T-talc.

Preparation of Samples

PP was premixed with 0.1 wt % B215 and 0.05 wt % NT-C. The mixture was compounded in a corotating twin-screw extruder [TE-20, D = 20 mm, L/D = 32/1, Coperion Keya (Nanjing) Machinery, Nanjing, China] and β-PP pellets were obtained. Then β-PP was mixed with 5 wt % PP-*g*-MAH and variable fractions of T-talc, ranging from 1 to 20 wt %. The total amount was 500 g. The mixture was compounded in the same corotating twin-screw extruder. The rates of feeding screw and main screw were 30 and 200 rpm, and the temperatures from the hopper to the die were 190, 200, 200, and190°C, respectively. The melt was cooled and pelletized.

To make a comparison, β-PP/T-talc and PP/T-talc composites were also prepared in a similar way, respectively.

A granule of composites was placed between two glass slides on a hot stage kept at 210°C for 5 min to allow the sample to melt completely and remove thermal history, and then squeezed on the top slide to form a film. Then, the film was put in a glycerin bath kept at 120°C for 30 min, and then quenched in ice water and dried at room temperature. The thickness of the samples after isothermal crystallization was about 0.5 mm for differential scanning calorimetry (DSC) and wide angle X-ray diffraction (WAXD) characterization, and 10–20 μm for polarized light microscopy (PLM) observation, respectively.

Differential Scanning Calorimetry Measurement

The melting and crystallization behaviors of isothermal crystallization samples were measured with a ZF-DSC-D2 DSC apparatus (Shanghai Zufa Industry, Shanghai, China) in a dry nitrogen atmosphere. The instrument was calibrated with pure indium, tin, and zinc for temperature and heat flow, respectively. All the samples were heated from room temperature to 210°C at a rate of 10°C/min, and held at 210°C for 5 min to eliminate the thermal history. Then, the melted samples were cooled down to 100°C at the rate of 10°C/min and held at 100°C for 5 min, finally reheated to 210°C at the rate of 10°C/min. Varga[34] reported the formation of pure β-iPP has an upper [T($\beta\alpha$) = 140–141°C] and lower limit temperatures [T($\alpha\beta$) = 105°C]. In order to eliminate the β–α transition below the T($\alpha\beta$), the final cooling temperature was set as 100°C.

The heat flow versus temperature was recorded and peak melting temperatures of α-PP ($T_{m,\ \alpha}$) and β-PP ($T_{m,\ \beta}$) were obtained from the melting curves. The onset (T_c^{on}) and peak (T_c^{P}) crystallization temperatures were obtained from the

cooling curves. The contents of β crystalline form (K_{DSC}) were calculated as follows:

$$K_{DSC} = [A_\beta/(A_\alpha + A_\beta)] \times 100\% \quad (1)$$

where A_α and A_β were the areas of α and β melting peaks, respectively.

During the non-isothermal crystallization kinetics measurements, about 5 mg of each sample was sealed into an aluminum crucible, heated from 50° to 210°C at 20°C/min, and held at 210°C for 5 min to remove the thermal history, then cooled to 50°C at the constant cooling rate of 5, 8, 10, and 15°C /min, respectively.

Wide Angle X-ray Diffraction Characterization

Wide Angle X-ray Diffraction (WAXD) diffraction patterns of isothermal crystallization samples were recorded in an X-ray diffractometer (ARLX'TRA, Thermo Electron Corporation) equipped with Ni-filtered Cu $K\alpha$ radiation ($\lambda = 1.54$ Å). Radial scans of intensity versus diffraction angle (2θ) were recorded in the range of 5–35°, with a scanning rate of 10°/min. The relative content of β crystalline form was measured in terms of K_{WAXD} proposed by Turner-Jones et al.[35]

$$K_{WAXD} = [H_{\beta1}/(H_{\beta1} + H_{\alpha1} + H_{\alpha2} + H_{\alpha3})] \times 100\% \quad (2)$$

where $H_{\alpha1}$, $H_{\alpha2}$, and $H_{\alpha3}$ were the heights (from the top of the peak to the background curve) of three strong α crystalline form peaks, (110), (040), and (130) at $2\theta = 14.1°$, 16.9°, and 18.8°, respectively; and $H_{\beta1}$ was the height of β crystalline form peak (300) at $2\theta = 16°$.

Polarized Light Microscopy (PLM) Observation

Spherulitic morphologies of the isothermal crystallization samples were observed in a polarized light microscope (LW-200-4JS, Shanghai LW Scientific, Shanghai, China) equipped with cross polars and a CCD camera. Pictures were captured and stored in a computer.

Scanning Electron Microscopy Observation

A scanning electron microscopy (SEM; SSX-550, Shimadzu, Japan) was used to observe the microstructures of the impact-fractured surfaces of selected specimens obtained after the impact testing. Prior to observation, the fresh fractured surfaces were sputtered with gold under vacuum.

Mechanical Measurement

Standard test specimens for mechanical characterization were injection-molded with a reciprocating-screw injection molding machine (CJ80M3V, Chen De Plastics Machinery, Foshan, China) at a temperature range of 190–200°C and an injection pressure of 70 MPa. The tensile strength and flexural modulus tests were carried out on an electromechanical universal testing machine (CMT5254, Shenzhen SANS Testing Machine, Shenzhen, China) according to ISO527-2/1BA: 1996 and ISO178: 2003, respectively. The testing speeds for tensile strength and flexural modulus were 50 and 2 mm/min, respectively. The Izod notched impact strengths were tested on a pendulum impact testing machine (MZ2056, Jiangdu Mingzhu Testing Machine Factory, Jiangdu, China) according to ISO180/A: 2000. Before measurement, specimens were notched on a plastic specimen notcher (MZ2061, Jiangdu Mingzhu Testing Machine Factory, Jiangdu, China).

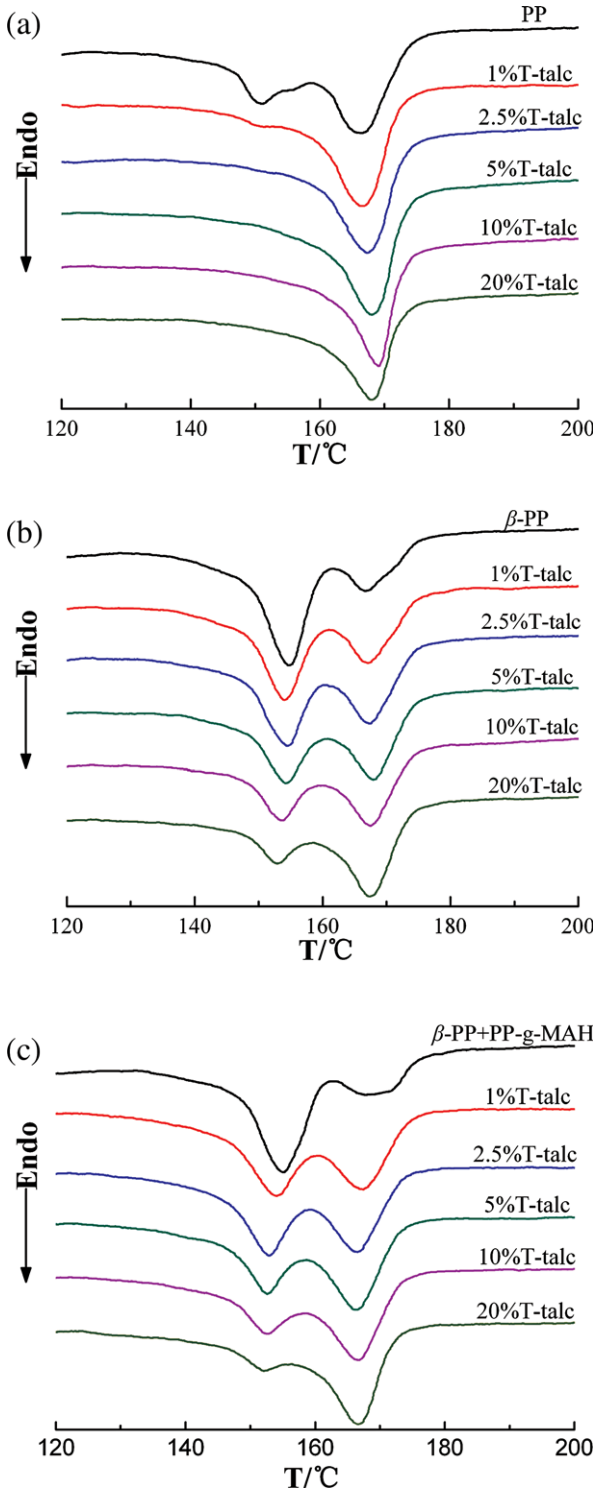

Figure 1. DSC first heating curves of isothermal crystallization samples. (a) PP/T-talc composites, (b) β-PP/T-talc composites, and (c) β-PP/PP-*g*-MAH/T-talc composites. [Color figure can be viewed in the online issue, which is available at wileyonlinelibrary.com.]

RESULTS AND DISCUSSION

DSC Measurement

DSC melting curves of the isothermal crystallization samples are shown in Figures 1 and 2; the relevant parameters are shown in Table I. There are three peaks in the melting curve of neat PP.

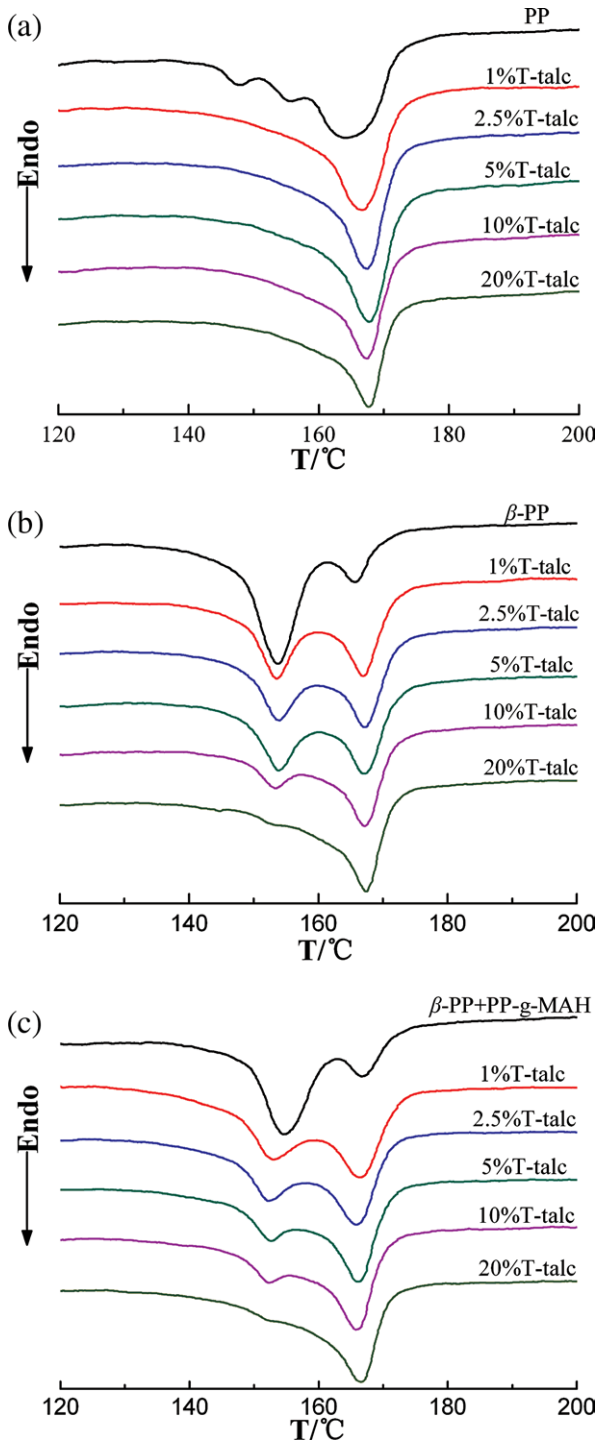

Figure 2. DSC second heating curves of isothermal crystallization samples. (a) PP/T-talc composites, (b) β-PP/T-talc composites, and (c) β-PP/PP-*g*-MAH/T-talc composites. [Color figure can be viewed in the online issue, which is available at wileyonlinelibrary.com.]

The peak at 166.3°C corresponds to the melting of α-phase.[36]. Double peaks at 150.7 and 155.8°C are attributed to melting of the β_1 and β_2 phases, results from $\beta_1\beta_2$ recrystallization. This is a structure perfection process within β-phase, which is superimposed on the melting of the original crystals.[37] For PP/T-talc composites, in the first heating process, double β-peaks of pure PP become a very small β-peak when 1 wt % T-talc was added. No β-phase peaks appear as further increasing concentration of T-talc. Obvious double β-peaks of pure PP also appear, but no β-phase peaks appear with addition of T-talc in the second heating process. The first and second heating curves are different because of the different thermal history that the samples suffered. In Table I, K_{DSC} of PP/T-talc composites decreases noticeably from 41.9% to 18.8% with the addition of 1 wt % T-talc and even to 0% as further addition of fillers in the first heating. It indicates that T-talc suppresses the formation of β-phase. However, in the second heating, K_{DSC} decreases directly to 0% with initial addition of 1 wt % T-talc. Because isothermal crystallization condition is favor of the β-crystals formation, 18.8% β-phase content can be obtained in the first heating process for PP/1 wt % T-talc composite sample which were isothermally crystallized at 120°C for 30 min.

Double α-peaks at about 167 and 172°C appear besides the big β peak in the first heating process of β-PP sample [Figure 1(b)]. The lower peak (α_1) is attributed to the melting of the original α-modification, whereas the shoulder peak at higher temperature (α_2) is due to the melting of the α-modification formed during the $\beta\alpha$-recrystallization.[38] The shoulder peak α_2 for β-PP/T-talc composites disappears. With the addition of T-talc, the areas of the α melting peaks augment, while the areas of the β peaks diminish noticeably in the twice heating. The values of K_{DSC} diminish continuously with increasing contents of T-talc in the twice heating (Table I). It is found that K_{DSC} values in the first heating are larger than those in the second heating except the β-PP. The difference owes to the $\beta\alpha$-recrystallization during the cooling.

Double α-peaks also appear after the addition of PP-*g*-MAH into β-PP in the first heating process [Figure 1(c)]. Similarly, the double α-peaks disappear and become a sharper peak in the second heating. In addition, there are also single β peaks in the twice heating curves of β-PP/PP-*g*-MAH/T-talc composites but the areas of these β peaks are smaller than those of β-PP/T-talc composites. The trend of K_{DSC} is similar to that of non-compatibilized β-PP composite in twice heating processes. K_{DSC} is lower than that of β-PP/T-talc composites, indicating PP-*g*-MAH is unfavorable to the formation of β-form PP. PP-*g*-MA with polar functional group might capture β-nucleating agent, reducing the nucleator content in PP.[39]

The cooling curves of the isothermal crystallization samples are presented in Figure 3 and the relevant parameters are listed in Table I. Only a single crystallization peak is observed for each curve, meaning the simultaneous crystallization of β-phase, and α-phase during the cooling process. It is clear that T_c^{on} and T_c^{P} shift to higher temperatures after the addition of T-talc [Figure 3(a)]. This confirms that T-talc acts as a nucleating agent, as previously mentioned in the literatures.[7,40]

Table I. DSC Parameters of Isothermal Crystallization Samples

		The first heating					The second heating				Cooling	
Sample	T-talc (wt %)	$T_{m,\alpha1}$ (°C)	$T_{m,\alpha2}$ (°C)	$T_{m,\beta1}$ (°C)	$T_{m,\beta2}$ (°C)	K_{DSC} (%)	$T_{m,\alpha}$ (°C)	$T_{m,\beta1}$ (°C)	$T_{m,\beta2}$ (°C)	K_{DSC} (%)	T_c^P (°C)	T_c^{on} (°C)
PP	0	166.3	–	150.7	155.8	41.9	164.4	147.7	155.4	34.1	104.7	113.4
	1	166.8	–	150.1	–	18.8	166.6	–	–	0	114.7	119.6
	2.5	167.5	–	–	–	0	167.3	–	–	0	117.8	122.5
	5	168.3	–	–	–	0	167.7	–	–	0	118.1	122.8
	10	169.0	–	–	–	0	167.3	–	–	0	119.4	124.0
	20	168.1	–	–	–	0	167.7	–	–	0	120.8	125.4
β-PP	0	166.8	172.0	154.7	–	72.2	166.7	154.2	–	74.6	117.9	122.1
	1	166.9	–	154.1	–	61.3	167.0	153.7	–	53.5	118.6	123.1
	2.5	167.3	–	154.8	–	56.8	167.3	154.1	–	51.1	118.5	123.1
	5	167.9	–	154.4	–	54.0	167.2	153.9	–	50.5	118.8	123.0
	10	167.5	–	153.5	–	50.2	167.3	153.3	–	32.3	119.7	124.0
	20	167.3	–	153.0	–	39.0	167.2	152.4	–	21.9	120.7	125.3
β-PP/PP-*g*-MAH	0	167.5	171.3	155.1	–	70.3	167.0	154.6	–	72.7	116.9	121.4
	1	167.3	–	154.1	–	56.0	166.4	153.0	–	50.7	116.2	120.9
	2.5	166.4	–	153.0	–	53.1	165.9	152.3	–	46.3	116.6	121.0
	5	166.3	–	152.6	–	47.0	166.1	152.8	–	34.2	117.6	122.0
	10	166.6	–	152.4	–	41.7	165.9	152.3	–	28.9	117.9	122.6
	20	166.7	–	152.3	–	25.6	166.4	152.1	–	19.7	118.9	123.7

With the presence of NT-C in PP, T_c^{on}, and T_c^P shift to higher temperatures, and the increments for β-PP/T-talc composites are larger than those of PP/T-talc composites except the 20 wt % loading. It indicates that both T-talc and NT-C promote the crystallization rate of PP, but the effect of NT-C is superior to that of T-talc. Shi and Dou[12] also found T_c^{on} and T_c^P of iPP shifted to higher temperatures after the addition of β nucleating agents. Varga[37] showed that β-iPP crystallized in a temperature range of 10–15°C higher than its non-nucleated counterpart.

With the addition of PP-*g*-MAH into β-PP, T_c^{on}, and T_c^P move to lower temperature and these temperatures of β-PP/PP-*g*-MAH/T-talc composites are lower than those of β-PP/T-talc composites. Thus, PP-*g*-MAH has a faint negative effect on the crystallization rate of β-PP. Although the concentration of T-talc increases in β-PP/T-talc or β-PP/PP-*g*-MAH/T-talc composites, the increments of T_c^{on} and T_c^P are limited.

WAXD Characterization

WAXD patterns of isothermal crystallization samples are shown in Figure 4. The K_{WAXD} values calculated by eq. (2) are listed in Table II. The diffraction peaks of pure PP located at $2\theta = 14.1°$, 16.9°, 18.8°, 20.9°, and 21.7°, correspond to the reflection planes of (110), (040), (130), (111), and (041) of α-phase, respectively, and the characteristic peak at $2\theta = 16°$ corresponds to the (300) plane of β-phase.[3] The intensity of β (300) peak decreases sharply with the addition of 1 wt % T-talc, accompanied with K_{WAXD} value decreases from 41.0% (pure PP) to 13.0%. And, β (300) peak disappears when 5 wt % T-talc is added, indicating that T-talc restrains the formation of β-crystal. The intensity of β (300) peak increases dramatically after the addition of NT-C and the K_{WAXD} value is 78.9%. The K_{WAXD} values of β-PP/T-talc composites diminish continuously along with T-talc content, but they are higher than those of PP/T-talc composites at each loading.

For β-PP/PP-*g*-MAH/T-talc composites, K_{WAXD} value decreases to 75.9% after the addition of PP-*g*-MAH into β-PP. When T-talc fillers were added, a further decrease of K_{WAXD} can be found, and K_{WAXD} values are lower than those of β-PP/T-talc composites, which is in agreement with the DSC results of isothermal crystallization samples in the first heating which underwent the same thermal history. Although double melting peaks appear in the first DSC heating curves of isothermal crystallization samples, there are not other crystal phases except α- and β-crystals in WAXD spectra.

PLM Observations

Figures 5–7 show the PLM micrograghs of isothermal crystallization samples. In Figure 5(a), the spherulitic morphology of the pure PP sample predominantly consists of α-spherulites, and the spherulitic size is about 70 μm. However, a few spherulites are bright and colored, indicating the presence of some β-spherulites,[4] which is in agreement with the results of DSC and WAXD. In comparison to the pure PP sample, the spherulitic size of PP decreases obviously with the presence of 1 wt % T-talc. The number of bright β-spherulites also decreases when T-talc loading increases, indicating that fillers suppress the formation of β-form. When NT-C is introduced into PP [Figure 6(a)], the spherulitic size of PP decreases so greatly that it is

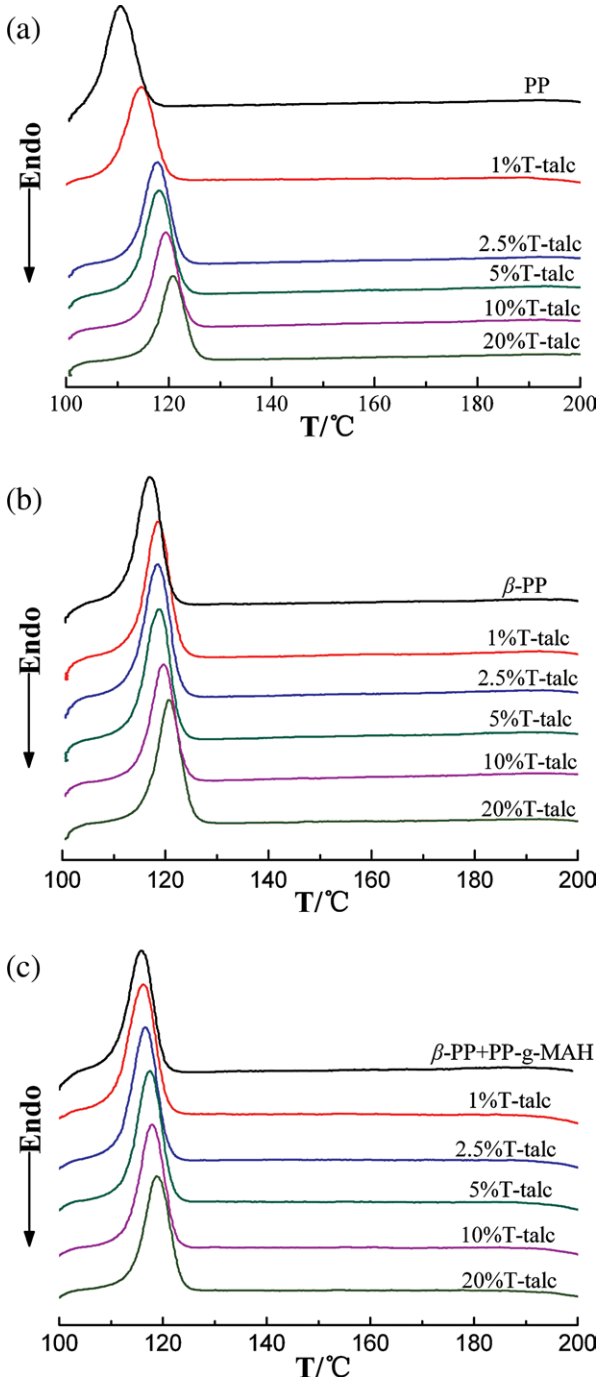

Figure 3. DSC cooling curves of isothermal crystallization samples. (a) PP/T-talc composites, (b) β-PP/T-talc composites, (c) β-PP/PP-*g*-MAH/T-talc composites. [Color figure can be viewed in the online issue, which is available at wileyonlinelibrary.com.]

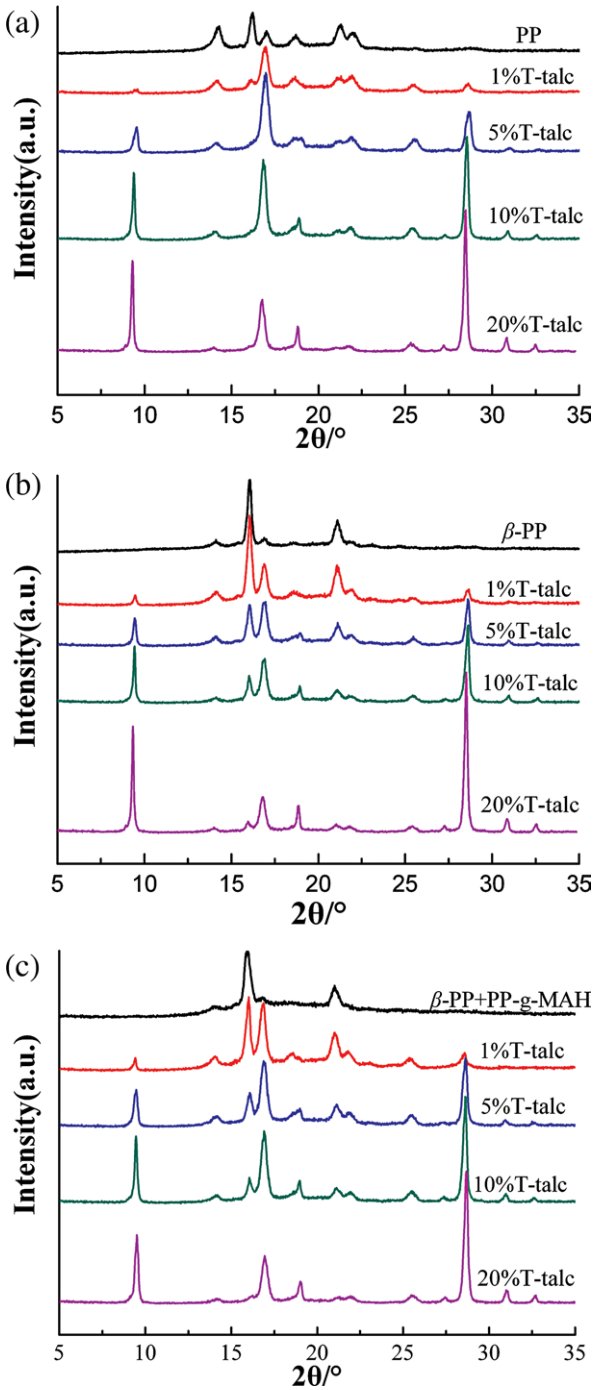

Figure 4. WAXD patterns of isothermal crystallization samples. (a) PP/T-talc composites, (b) β-PP/T-talc composites, and (c) β-PP/PP-*g*-MAH/T-talc composites. [Color figure can be viewed in the online issue, which is available at wileyonlinelibrary.com.]

hard to be figured out. The increasing T-talc content has no remarkable effect on spherulitic size but has a restrained effect on the β-spherulites contents in β-PP/T-talc composites. There is no obvious change of the spherulitic morphology in β-PP/PP-*g*-MAH composite [Figure 7(a)] compared to non-compatibilized composites. Likewise, the bright small β spherulites decrease monotonously with increasing content of T-talc content.

SEM Observations

SEM micrograghs of the fractured surfaces of the composites are presented in Figure 8. For PP/T-talc [99 wt %/1 wt %; Figure 8(a)], the relative smooth fractured surface is present and this indicates that little plastic deformation took place during the impact tests. Some T-talc particles are pulled out from the fractured surfaces during the impact process, leading to the

Applied Polymer SCIENCE

Table II. K_{WAXD} Values of Isothermal Crystallization Samples

Sample	T-talc (wt %)	K_{WAXD} (%)
PP	0	41.0
	1	13.0
	5	0
	10	0
	20	0
β-PP	0	78.9
	1	61.7
	5	40.5
	10	29.6
	20	12.6
β-PP/PP-*g*-MAH	0	75.9
	1	46.0
	5	26.9
	10	19.1
	20	8.4

formation of microvoids. For PP/T-talc [90 wt %/10 wt %; Figure 8(b)], some T-talc agglomerates can be found, meaning that the good distribution of T-talc particles is unavailable.

Compared with PP/T-talc composite, some microvoids can also be found in the fractured surface of *β*-PP/T-talc composite but the fractured surface is relatively coarse, indicating a slight plastic deformation. It may be related to higher content of *β*-phase and smaller spherulite size as proved by the results of WAXD, DSC, and PLM. Tjong et al.[41] reported that the fractured surface of α-PP is relatively smooth and is of a brittle appearance, whereas *β*-PP specimen has a rough surface and a grainy appearance. For 10 wt % T-talc content [Figure 8(d)], agglomerates can also be seen in the composite, which deteriorates the mechanical property as shown later. The orientation of T-talc particulates along the flow direction during injection molding is clearly seen. This particle organization is a consequence of the plate-like structure of talc and its motion in a viscous medium during the injection-molding process.[9]

Compared to *β*-PP/T-talc composite, the interface between PP and T-talc particles in *β*-PP/PP-*g*-MAH/T-talc composite is blurry and the amount of microvoids visibly decreases, which result in a better compatibility and greater adhesion. For 10 wt % T-talc content, the agglomerate can hardly be found in Figure 8(f). It owes to better compatibility between T-talc and the matrix. The presence of microfibrils exhibits shear yielding of the matrix (in black circles).

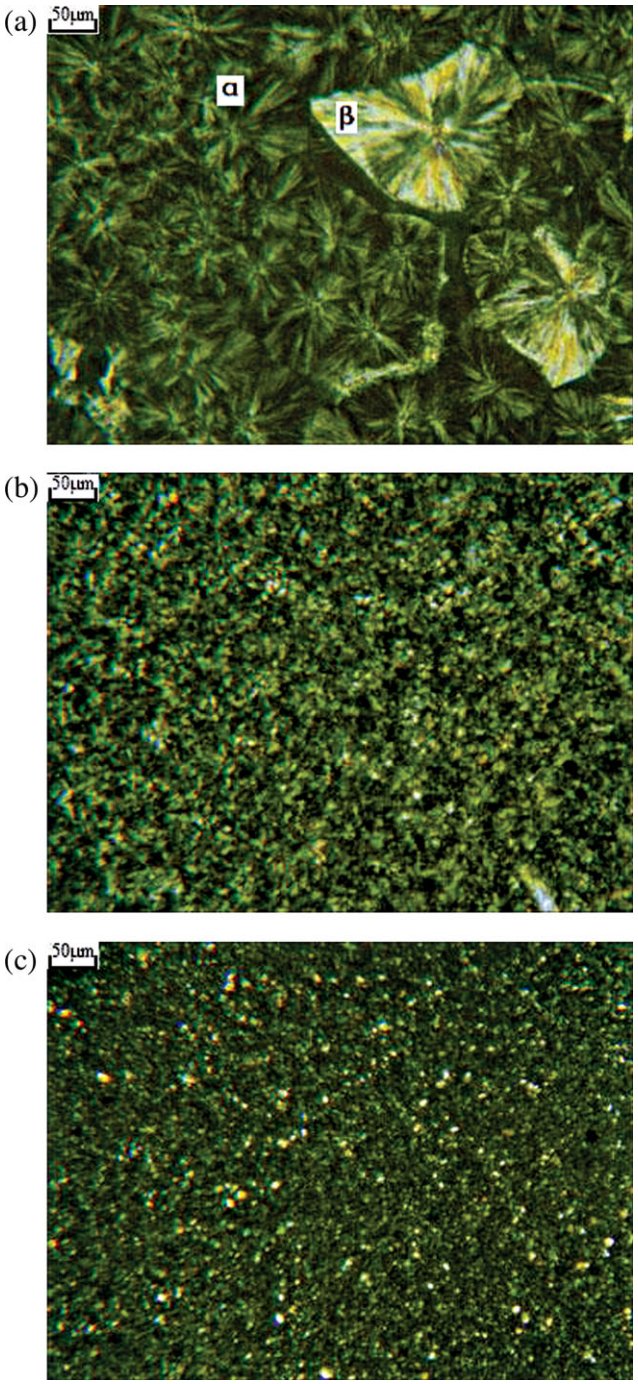

Figure 5. PLM photographs of PP/T-talc isothermal crystallization samples. (a) Pure PP (b) 1 wt % T-talc, and (c) 10 wt % T-talc. [Color figure can be viewed in the online issue, which is available at wileyonlinelibrary.com.]

Mechanical Measurement

Figure 9(a) presents the effect of T-talc content on the Izod notched impact strength of the composites. When T-talc is added into the pure PP, the Izod notched impact strength increases somewhat until 5 wt % T-talc and then it decreases gradually. It demonstrates that surface treated talc particles possess toughening effects which had been reported by other researchers.[9,10] With the addition of nucleating agent (NT-C), the impact strength of the pure PP is improved. It is attributed to the increased content of small *β*-spherulites. It was reported that *β*-PP is much tougher than α-PP because *β*-spherulites exhibit curved lamellae and sheaf-like structure.[6] As can be seen, initial incorporation of T-talc leads to the increase in the impact strength of *β*-PP/T-talc composites. The maximum impact strength (9.22 kJ/m^2) is obtained at 2.5 wt % T-talc. The

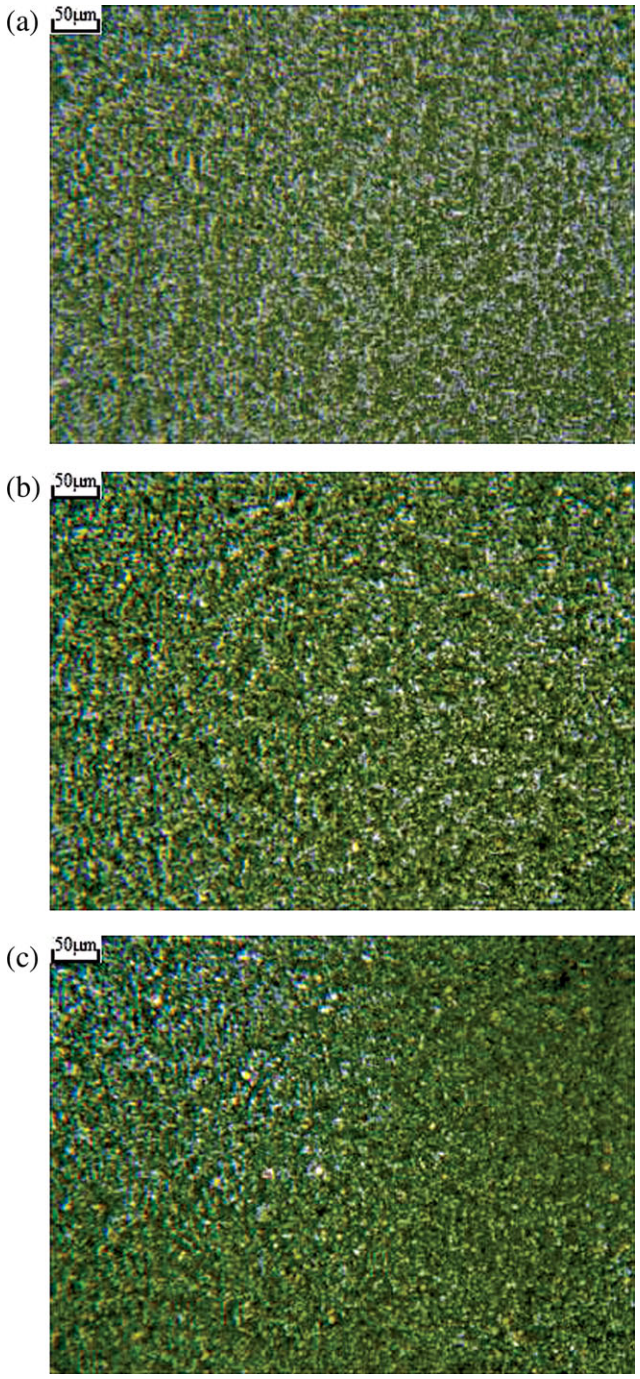

Figure 6. PLM photographs of β-PP/T-talc isothermal crystallization samples. (a) β-PP (b) 1 wt % T-talc, and (c) 10 wt % T-talc. [Color figure can be viewed in the online issue, which is available at wileyonlinelibrary.com.]

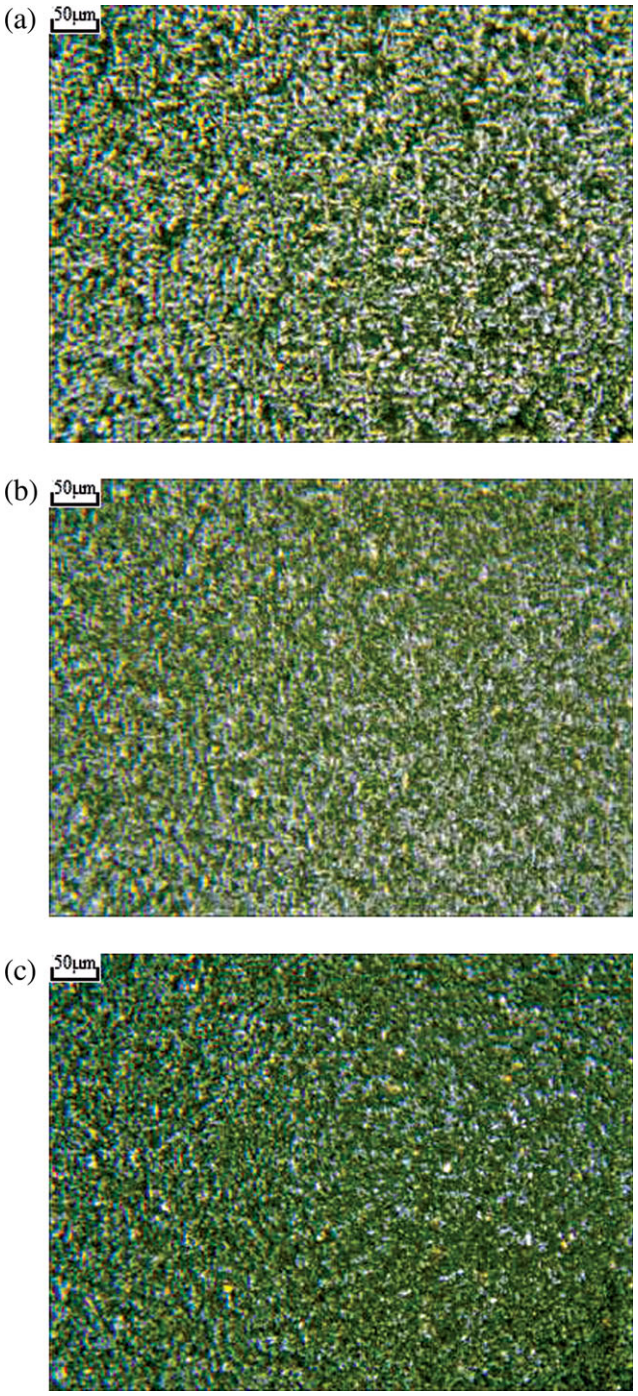

Figure 7. PLM photographs of β-PP/PP-*g*-MAH/T-talc isothermal crystallization samples. (a) β-PP/PP-*g*-MAH, (b) 1 wt % T-talc, and (c) 10 wt % T-talc. [Color figure can be viewed in the online issue, which is available at wileyonlinelibrary.com.]

notched impact strength of β-PP/T-talc composites is higher than that of PP/T-talc composites at each loading. The better toughening effect owes to the higher content of β-phase and much smaller spherulites in β-PP/T-talc composites as proved by the results of DSC, WAXD, and PLM. With the addition of PP-*g*-MAH into β-PP, a further increase in the impact strength is obtained and it increases from 7.17 kJ/m^2 (β-PP) to 9.03 kJ/m^2 (β-PP/PP-*g*-MAH). Incorporation of small amount of T-talc ($\leq$2.5 wt %) into β-PP/PP-*g*-MAH can also benefit the impact strength and it is higher than that of corresponding β-PP/T-talc composites. Compared to non-compatibilized composites, PP-*g*-MAH reduces the β-phase content as shown in the results of DSC and WAXD, but it promotes the compatibility and adhesion between T-talc and PP matrix as proved by SEM. However,

Applied Polymer SCIENCE

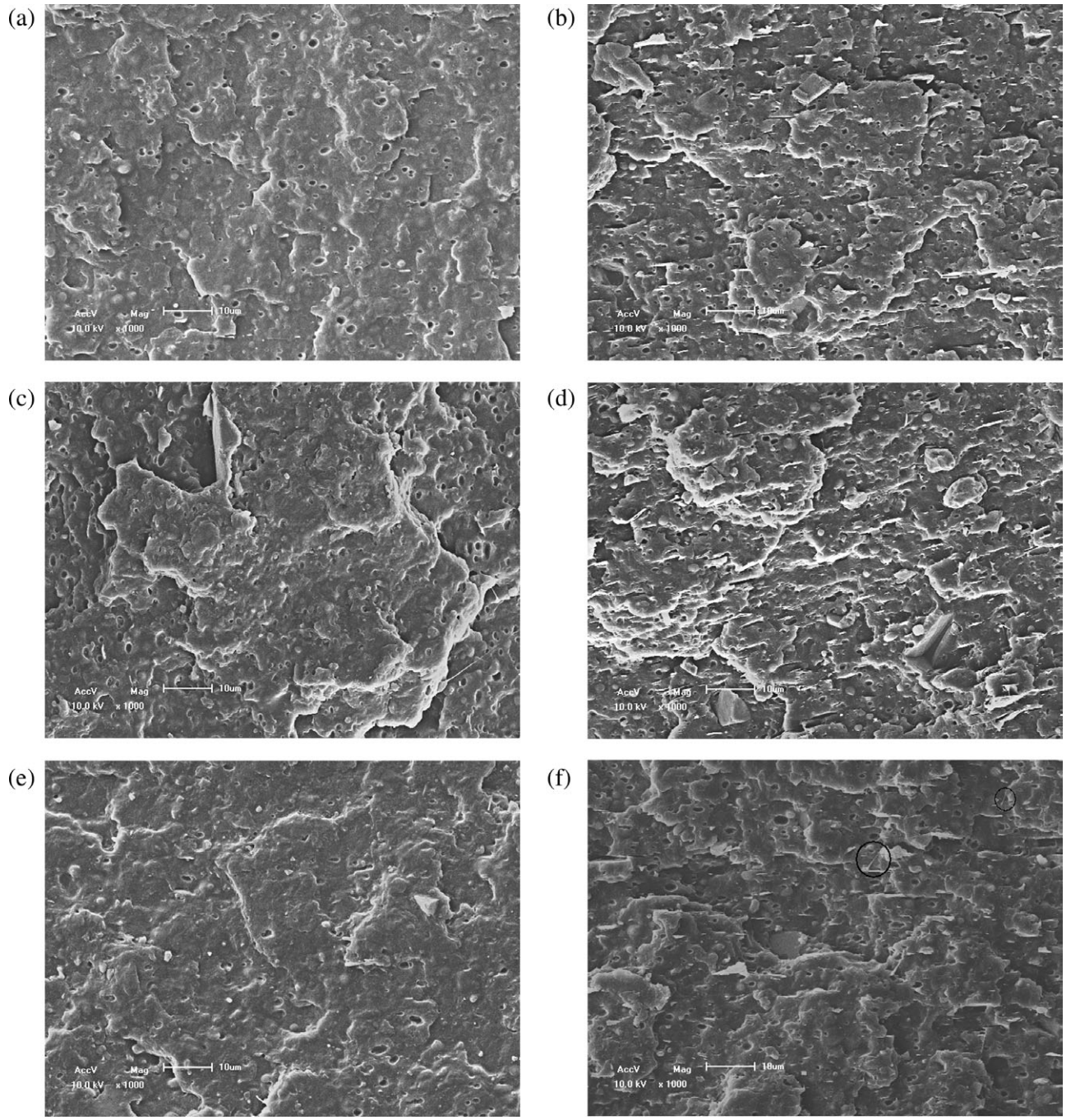

Figure 8. SEM micrographs of fractured surfaces of the composites. (a) PP/T-talc (99 wt %/1 wt %) (b) PP/T-talc (90 wt %/10 wt %), (c) *β*-PP/T-talc (99 wt %/1 wt %), (d) *β*-PP/ T-talc (90 wt %/10 wt %), (e) *β*-PP/PP-*g*-MAH/T-talc (94 wt %/5 wt %/1 wt %), and (f) *β*-PP/PP-*g*-MAH/T-talc (85 wt %/5 wt %/10 wt %).

when the concentration of T-talc is high (beyond 2.5 wt %), the inorganic filler effect will become the dominant factor, which suppresses the toughening effect of *β*-spherulites; thus, the notched impacted strengths of *β*-PP/T-talc and *β*-PP/PP-*g*-MAH/T-talc composites decrease at higher contents of T-talc, but the values are still higher than those of PP/T-talc composites.

The flexural moduli of the composites are shown in Figure 9(b). With increasing T-talc loading, the flexural modulus increases almost linearly. It is well-known that the incorporation of talc improves the stiffness of plastic matrices. The enhancement can be attributed to the high aspect ratio and particle orientation of T-talc. The curve of *β*-PP/T-talc composites has a similar trend as that of PP/T-talc composites, but the latter is higher than the former at each loading. Incorporation of PP-*g*-MAH increases the flexural moduli of *β*-PP/T-talc composites but it is still lower that of PP/T-talc composites at each loading. Compared with α-spherulites consisting of aggregates of

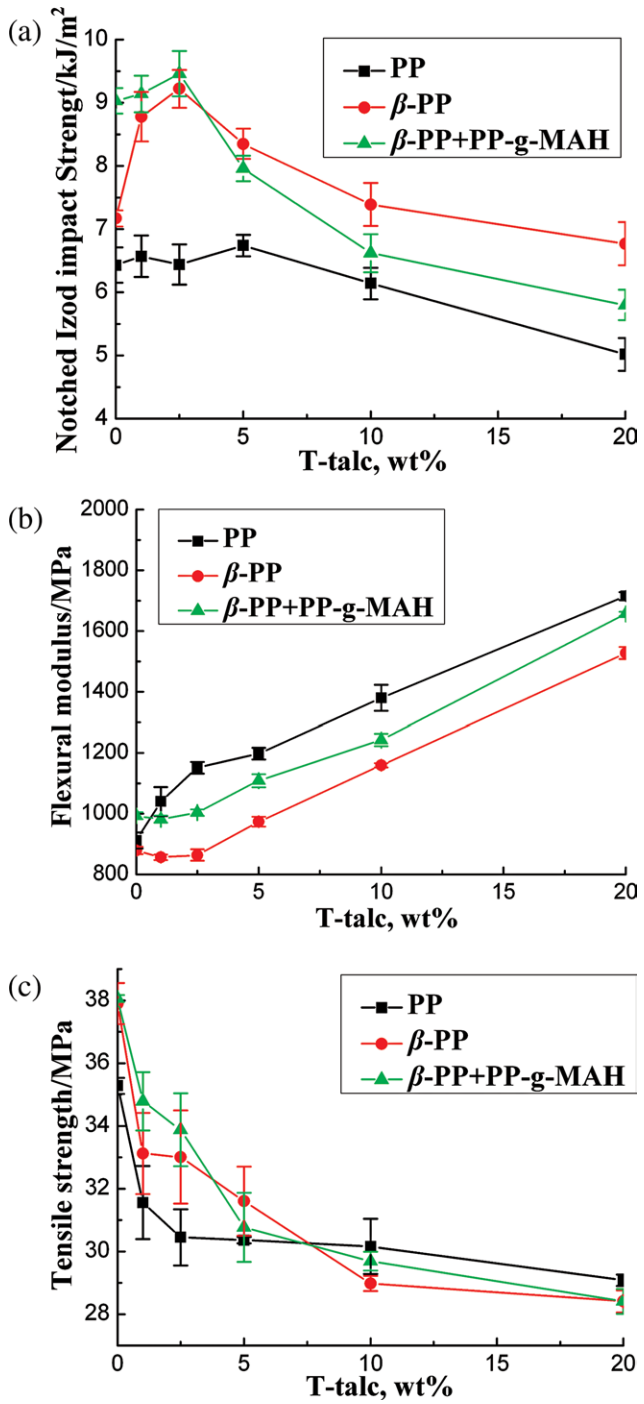

Figure 9. Mechanical properties of the composites. (a) Izod notched impact strength, (b) flexural modulus, and (c) tensile strength.[Color figure can be viewed in the online issue, which is available at wileyonlinelibrary.com.]

lamellae that radiate from the center outward, β-spherulites exhibit a classical sheaf-like structure having interleaving lamellae at their boundaries.[41,42] This structural difference results in β-PP having lower values of flexural modulus. β-PP/T-talc composites contain higher β-phases than the corresponding PP/T-talc and β-PP/PP-*g*-MAH/T-talc composites, thus the flexural moduli of β-PP/T-talc composites are lowest.

The tensile strength reflects both the properties of the polypropylene matrix and the presence of T-talc. In Figure 9(c), for PP/T-talc composites, there is a significant decrease of tensile strength with increasing content of T-talc. The reduction of the strength of the composites filled with T-talc, which agreed with the results obtained by Leong et al.[9] and Ai Wah et al.[10], was due to the role of the titanate coupling agent in acting as a plasticizer in the filled system. The tensile strength of β-PP/ T-talc and β-PP/PP-*g*-MAH/ T-talc composites have similar trends but it is higher than that of PP/T-talc composites when T-talc content is ≤5 wt %. It owes to higher content of β-phase in β-PP composites as proved by the results of DSC and WAXD. β-PP possesses higher ultimate tensile strength in comparison with α-PP, because of the β to α transition occurring in the tensile process.[34] With the presence of PP-*g*-MAH, the tensile strength is higher that of β-PP/T-talc composites as initial addition of T-talc (below 5 wt %) because of a better compatibility and filler-matrix adhesion. The positive effect of PP-*g*-MAH on the tensile strength is also found by other researchers.[1,43]

Non-isothermal Crystallization Behavior

Non-isothermal crystallization exotherms are depicted in Figure 10, and the T_c^P values for all samples are shown in Table III. As the cooling rate increases, exothermic trace becomes wider and shifts to low temperature for all samples. When the cooling rate increases from 5°C/min to 20°C/min, T_c^P of PP, β-PP, β-PP/T-talc (90 wt %/10 wt %), and β-PP/PP-*g*-MAH/T-talc (85 wt %/5 wt %/10 wt %) samples decrease from 108.9°C, 122.3°C, 123.6°C, and 122.8°C to 100.6°C, 114.0°C, 114.6°C, and 114.1°C, respectively. At a lower cooling rate, polymer chain has enough time to transfer from the melt to the surface of the crystal, so crystallization can occur at higher temperature. It can be seen from Table III that the order of T_c^P at all cooling rate is ranked as: β-PP/T-talc (90 wt %/10 wt %) > β-PP/PP-*g*-MAH/T-talc (85 wt %/5 wt %/10 wt %) > β-PP > PP. This implies that both β-nucleator and T-talc act as nucleating agents and promote the crystallization of PP. However, T_c^P decreases slightly with the addition of PP-*g*-MAH into β-PP/T-talc composites. It demonstrates that PP-*g*-MAH is ineffective in promoting the crystallization of β-PP.

The rate of evolution of the enthalpy of crystallization with temperature dH_c/dT for the PP crystallization could be measured from the DSC traces. Integration of dH_c/dT in the given range of crystallization temperature would result in the relative crystallinity (X_t) of PP at any temperature:

$$X_t = \frac{\int_{T_{on}}^{T} (dH_c/dT)dT}{\int_{T_{on}}^{T_\infty} (dH_c/dT)dT} \quad (3)$$

where T_{on}, T, and T_∞ are the initial, arbitrary, and final crystallization temperature, respectively. The crystallization temperatures during cooling can be converted to crystallization time:

$$t = (T_0 - T)/D \quad (4)$$

where D is the cooling rate and T_0 is the initial temperature. The transformation from T to t can be performed using a constant cooling rate.

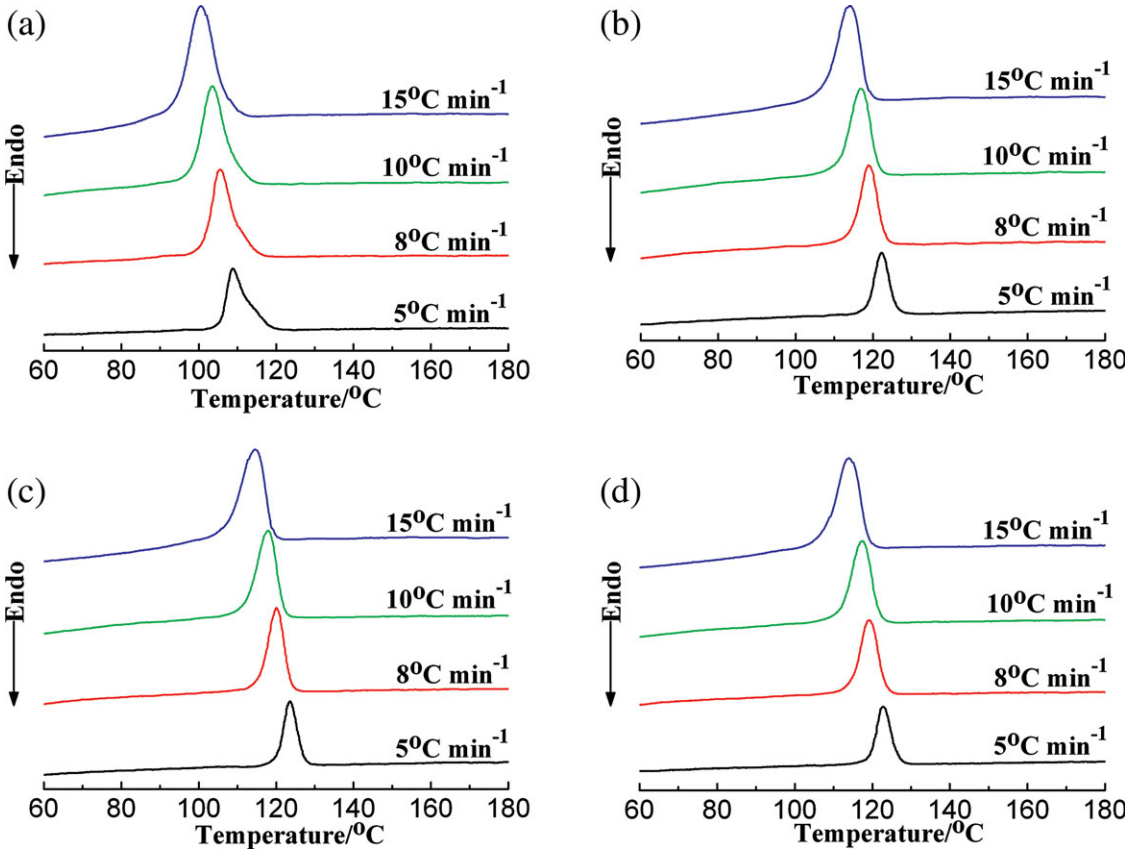

Figure 10. Non-isothermal crystallization exotherms of samples. (a) PP, (b) *β*-PP, (c) *β*-PP/T-talc (90 wt %/10 wt %), and (d) *β*-PP/PP-*g*-MAH/T-talc (85 wt %/5 wt %/10 wt %).[Color figure can be viewed in the online issue, which is available at wileyonlinelibrary.com.]

Figure 11 shows the relative crystallinity versus time curves of PP, *β*-PP, *β*-PP/T-talc (90 wt%/10 wt%), and *β*-PP/PP-*g*-MAH/T-talc (85 wt%/5 wt%/10 wt%) samples, respectively. Crystallization times with 50% relative crystallinity ($t_{1/2}$) can be obtained from Figure 11 and are listed in Table III. For all samples, $t_{1/2}$ decreases with increasing cooling rate, indicating that crystallization rate increases with increasing cooling rate. When the cooling rate increases from 5°C/min to 20°C/min, $t_{1/2}$ values of PP, *β*-PP, *β*-PP/T-talc (90 wt%/10 wt%), and *β*-PP/PP-*g*-MAH/T-talc (85 wt%/5 wt%/10 wt%) samples decreases from 2.78, 1.94, 1.66, and 1.67 min to 0.96, 0.65, 0.55, and 0.64 min, respectively. At a given cooling rate, the order of $t_{1/2}$ values ranks as: *β*-PP/T-talc (90 wt%/10 wt%) < *β*-PP/PP-*g*-MAH/T-talc (85 wt%/5 wt%/10 wt%) < *β*-PP < PP, which is accordance with the order of T_c^P as discussed above. It suggests that the addition of nucleating agent and T-talc accelerate crystallization rate but PP-*g*-MAH has a slight negative effect on crystallization rate of *β*-PP.

Non-isothermal Crystallization Kinetics

A modified Avrami equation proposed by Jeziorny could be used to analyze the non-isothermal crystallization kinetics of PP.[44]

$$1 - X_t = \exp(-Z_t t^n) \tag{5}$$

$$\lg[-\ln(1 - X_t)] = n \lg t + \lg Z_t \tag{6}$$

where X_t is the relative crystallinity at arbitrary time t. Z_t and n are the rate constant of crystallization and Avrami exponent,

Table III. T_c^P and $t_{1/2}$ of the Samples

Cooling rate (°C/min)	PP		β-PP		β-PP/T-talc (90 wt %/10 wt %)		β-PP/PP-*g*-MAH/T-talc (85 wt %/5 wt %/10 wt %)	
	T_c^P (°C)	$t_{1/2}$ (min)	T_c^P (°C)	$t_{1/2}$ (min)	T_c^P (°C)	$t_{1/2}$ (min)	T_c^P (°C)	$t_{1/2}$ (min)
5	108.9	2.78	122.3	1.94	123.6	1.66	122.8	1.67
8	105.7	1.70	118.9	1.15	120.2	1.00	119.2	1.08
10	103.6	1.34	116.9	0.98	117.9	0.82	117.5	0.89
15	100.6	0.96	114.0	0.65	114.6	0.55	114.1	0.64

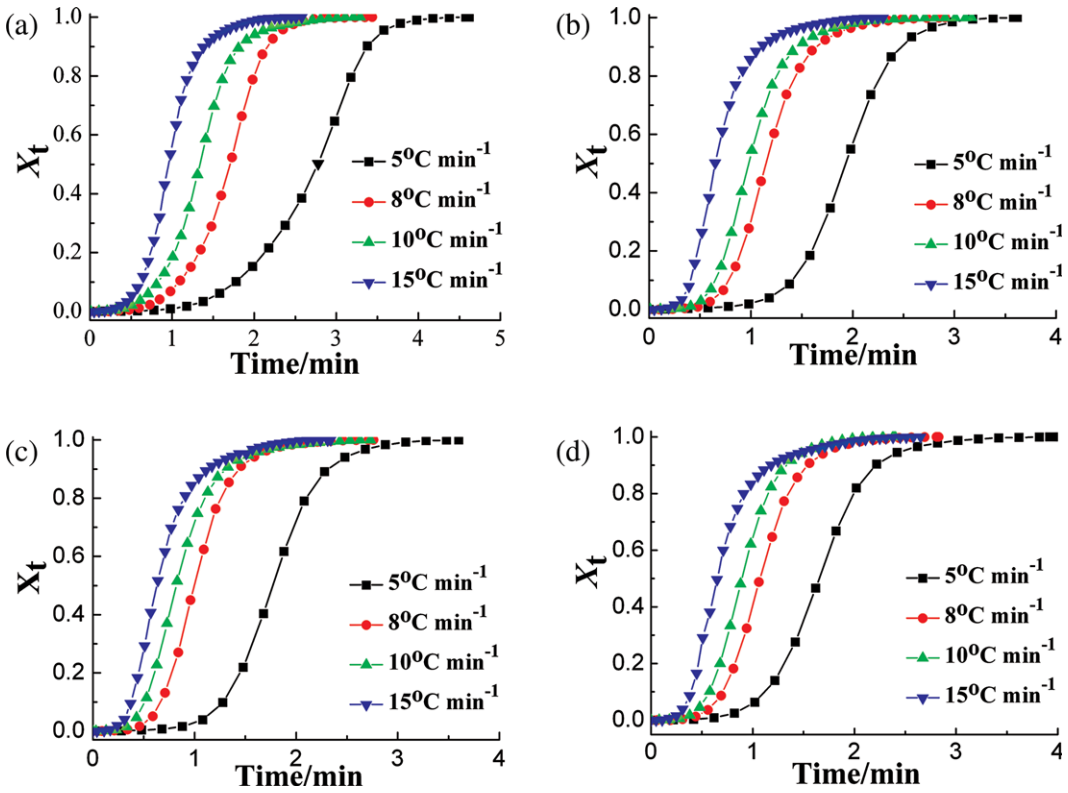

Figure 11. X_t versus time for samples. (a) PP, (b) β-PP, (c) β-PP/T-talc (90 wt %/10 wt %), and (d) β-PP/PP-*g*-MAH/T-talc (85 wt %/5 wt %/10 wt %).[Color figure can be viewed in the online issue, which is available at wileyonlinelibrary.com.]

respectively. The value of $\ln Z_t$ should be modified with the cooling rate to analyze non-isothermal crystallization process:

$$\lg Z_C = \lg Z_t / D \tag{7}$$

Ozawa extended Avrami equation to describe non-isothermal crystallization process. According to Ozawa's method, the relative crystallinity at temperature T amounts to[40]:

$$1 - X_t = \exp(-K(T)/D^n) \tag{8}$$

where $K(T)$ is the crystallization rate constant, n is the Ozawa index or Avrami exponent, which depends on the type of nucleation and growth dimensions.

Mo and coworkers successfully combined Ozawa's and Avrami's equations[45]:

$$\lg D = \lg F(T) - \alpha \lg t \tag{9}$$

$$F(T) = [K^*/Z_t]^{1/m} \tag{10}$$

$$\alpha = n/m \tag{11}$$

where n is the Avrami exponent, m is the Ozawa exponent, K^* is the cooling function of crystallization temperature in Ozawa's equation, and $F(T)$ is the value of the cooling rate to be chosen at a unit crystallization time when the system had the same crystallinity.

After fitting our experimental results with Jeziorny's method, Ozawa equation, and Mo's method, respectively, we found that Jeziorny's and Mo's methods can satisfactorily describe the non-isothermal crystallization behavior of the samples.

Jeziorny's Method

Figure 12 shows the curves of $\ln[-\ln(1 - X_t)]$ versus $\ln t$ for PP, β-PP, β-PP/T-talc (90 wt%/10 wt%) and β-PP/PP-*g*-MAH/T-talc (85 wt%/5 wt%/10 wt%) samples. The crystallization parameters of these samples are summarized in Table IV. According to the values of r^2, significant linear correlations between $\ln[-\ln(1 - X_t)]$ and $\ln t$ are observed for all samples, which means that the non-isothermal crystallization of PP, β-PP, β-PP/T-talc (90 wt%/10 wt%) and β-PP/PP-*g*-MAH/T-talc (85 wt%/5 wt%/10 wt%) samples can be well described by Jeziorny's method. For all the samples, Z_c increases with the increasing cooling rate, while $t_{1/2}$ shows the opposite trend, indicating that the crystallization rate increases with the increasing cooling rate. In comparison with PP and β-PP, Z_c of β-PP/T-talc (90 wt%/10 wt%) and β-PP/PP-*g*-MAH/T-talc (85 wt%/5 wt%/10 wt%) samples is observably larger at a given cooling rate. At the same time, for β-PP/T-talc (90 wt%/10 wt%) sample, Z_c is slightly higher but $t_{1/2}$ is lower than that of β-PP/PP-*g*-MAH/T-talc (85 wt%/5 wt%/10 wt%) composite at a given cooling rate. It also demonstrates that NT-C and T-talc have a synergistic effect on accelerating the crystallization of PP but PP-*g*-MAH has a slight negative effect on the crystallization rate

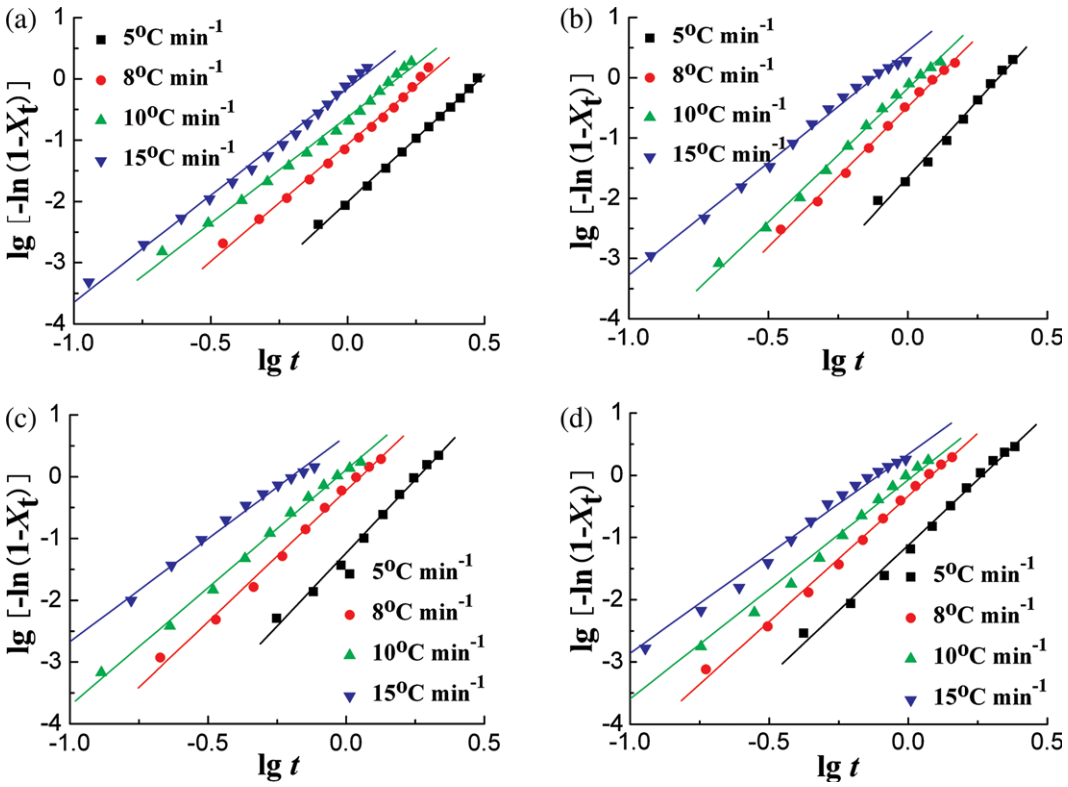

Figure 12. ln[−ln(1 − X_t)] versus ln$t$ for samples. (a) PP, (b) β-PP, (c) β-PP/T-talc (90 wt %/10 wt %), and (d) β-PP/PP-*g*-MAH/T-talc (85 wt %/5 wt %/10 wt %).[Color figure can be viewed in the online issue, which is available at wileyonlinelibrary.com.]

Table IV. Results of Jeziorny Analysis for Non-isothermal Crystallization of Samples

Samples	Avrami parameters	Cooling rate (°C/min)			
		5	8	10	15
PP	n	4.00	3.82	3.46	3.69
	Z_c	0.41	0.74	0.87	0.98
	r^2	0.9980	0.9944	0.9934	0.9943
β-PP	n	5.48	4.45	3.73	3.72
	Z_c	0.45	0.87	0.96	1.07
	r^2	0.9894	0.9966	0.9963	0.9948
β-PP/T-talc (90 wt %/10 wt %)	n	4.73	4.23	3.82	3.33
	Z_c	0.59	0.94	1.03	1.11
	r^2	0.9933	0.9938	0.9959	0.9943
β-PP/PP-*g*-MAH/T-talc (85 wt %/ 5 wt %/10 wt %)	n	4.41	4.03	3.62	3.24
	Z_c	0.57	0.91	1.00	1.09
	r^2	0.9927	0.9958	0.9885	0.9912

of β-PP/T-talc composite. The average values of Avrami exponent for PP, β-PP, β-PP/T-talc (90 wt%/10 wt%), and β-PP/PP-*g*-MAH/T-talc (85 wt%/5 wt%/10 wt%) samples are 3.74, 4.35, 4.03, and 3.83, respectively. The Avrami exponent n of β-PP increases compared with the pure PP, but decreases with the addition of 10 wt% T-talc and 5 wt% PP-*g*-MAH, suggesting that NT-C, T-talc, and PP-*g*-MAH have an influence on the mechanism of crystallization. It may be ascribed to the fact that NT-C and T-talc can act as nucleating agents for PP which has been discussed above. Moreover, according to the classical crystallization theory, as the $t_{1/2}$ decreases, PP crystallizes more quickly and at higher temperature.

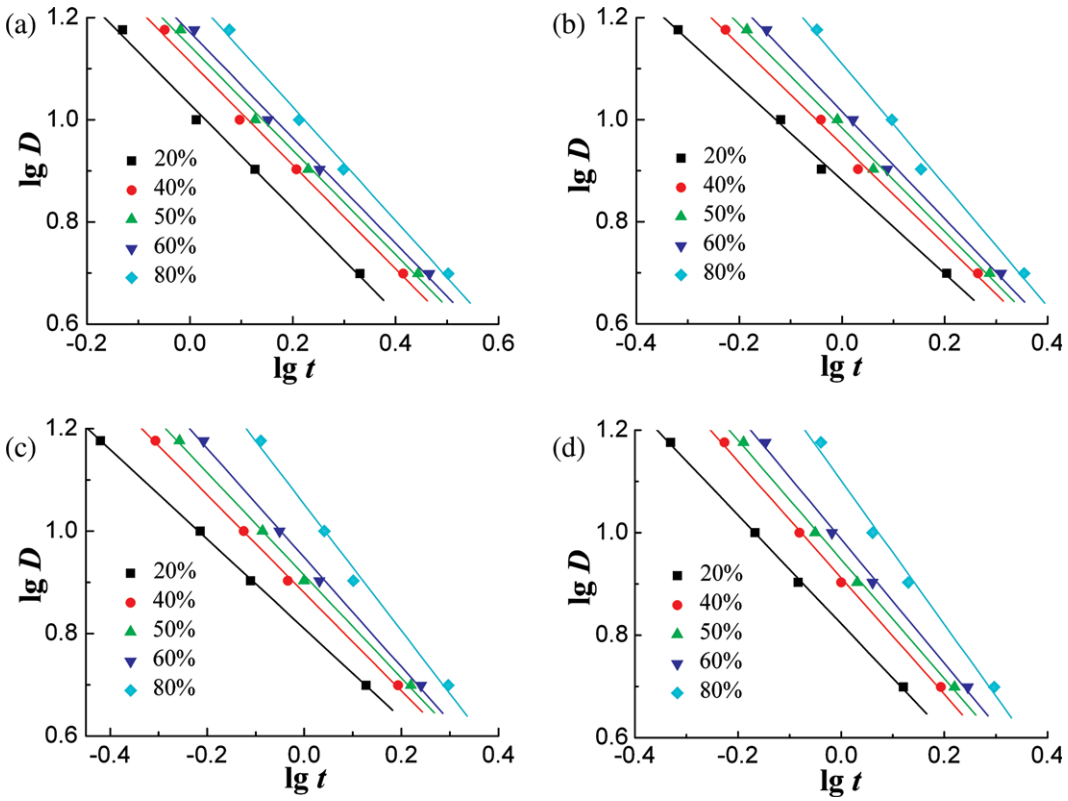

Figure 13. ln$D$ versus ln$t$ for samples. (a) PP, (b) β-PP, (c) β-PP/T-talc (90 wt %/10 wt %), and (d) β-PP/PP-g-MAH/T-talc (85 wt %/5 wt %/10 wt %).[Color figure can be viewed in the online issue, which is available at wileyonlinelibrary.com.]

In the classical Avrami equation, n may show values ranging from below 1 to far above 6. Any one value, whole or fractional, however, is not uniquely fixed to any one set of conditions. Additional information on nucleation, morphology, and possibly even mechanism is necessary to fully interpret the exponent n. For many macromolecules n is close to three and a picture of athermal heterogeneous nucleation followed by spherulitic growth is acceptable; others require $n = 4$, indicative of thermal nucleation, which is most often thermal heterogeneous nucleation followed by spherulitic growth. The also frequently observed exponent $n = 2$ could well be related to fibrillar or lamellar crystal growth following thermal or athermal nucleation, respectively.[46] Ding and Spruiell[47] proposed a modified Avrami equation to interpret the non-isothermal crystallization kinetics of PP using a power law nucleation rate function. The Avrami index n is composed of both a geometric index n^* and a nucleation index m. The latter may have wide latitude of values, depending on the nature of the nucleation process. This understanding provides a basis to better understand the many non-integer values of n occurring in the literature, as well as values that are greater than 4.

Mo's Method

Figure 13 shows linear relationships between lg$D$ and lg$t$ for various given crystallinities for the non-isothermal crystallization of PP, β-PP, β-PP/T-talc (90 wt%/10 wt%), and β-PP/PP-g-MAH/T-talc (85 wt%/5 wt%/10 wt%) composite samples. The values of α, $F(T)$, and r^2 are summarized in Table V. Obviously, according to the values of r^2, significant linear correlations between lg$D$ and lg$t$ are observed for all samples, implying the agreement of the experimental results with Mo's theoretical prediction. For each sample, $F(T)$ and α increase with the increasing relative crystallinity. α is in the order: β-PP/PP-g-MAH/T-talc (85 wt%/5 wt%/10 wt%) $>$ β-PP/T-talc (90 wt%/10 wt%) $>$ β-PP $>$ PP. Wang and Dou[48] also found the increase of α values after the addition of rosin-based nucleating agent into PP. For a certain degree of crystallinity, $F(T)$ for these samples is ranked as: PP $>$ β-PP $>$ β-PP/PP-g-MAH/T-talc (85 wt%/5 wt%/10 wt%) $>$ β-PP/ T-talc (90 wt%/10 wt%), indicating that faster cooling rates are needed for PP and β-PP than those of β-PP/T-talc (90 wt%/10 wt%) and β-PP/PP-g-MAH/T-talc (85 wt%/5 wt%/10 wt%) samples to obtain the same X_t. This indicates that the crystallization rate is increased with the addition NT-C and T-talc, which has also been proven above. At same time, a faster cooling rate is needed for β-PP/PP-g-MAH/T-talc (85 wt%/5 wt%/10 wt%) than that of β-PP/T-talc (90 wt%/10 wt%) composite to reach the same crystallinity, indicating that PP-g-MAH has a negative effect on crystallization rate of β-PP/T-talc composite. The result accords with those of Z_C and $t_{1/2}$.

Crystallization Activation Energy

Kissinger[49] proposed a method to determine the activation energy (ΔE) during non-isothermal crystallization process:

$$\mathrm{d}[\ln(D/T_P^2)]/\mathrm{d}(1/T_P) = -\Delta E/R \qquad (12)$$

Table V. Results of Mo's Analysis for Non-isothermal Crystallization of Samples

Sample	X_t (%)	α	$F(T)$	r^2
PP	20	1.00	10.74	0.9959
	40	1.01	13.02	0.9963
	50	1.01	13.96	0.9958
	60	1.02	14.85	0.9957
	80	1.11	17.68	0.9950
β-PP	20	0.98	7.62	0.9972
	40	1.01	8.94	0.9963
	50	1.03	9.63	0.9958
	60	1.05	10.38	0.9953
	80	1.19	12.87	0.9936
β-PP/T-talc (90 wt %/10 wt %)	20	0.96	6.45	0.9998
	40	1.02	7.57	0.9991
	50	1.04	8.20	0.9986
	60	1.06	8.88	0.9980
	80	1.23	11.28	0.9922
β-PP/PP-*g*-MAH/T-talc (85 wt %/5 wt %/10 wt %)	20	1.06	6.64	0.9992
	40	1.14	8.17	0.9985
	50	1.16	8.87	0.9981
	60	1.21	9.71	0.9967
	80	1.40	12.26	0.9910

where R is the gas constant. ΔE can be obtained from the slope in the plot of ln (D/T_p^2) versus $1/T_p$.

The plots of ln (D/T_p^2) against $1/T_p$ of samples are shown in Figure 14. It can be seen that good linear relations are obtained. From the slopes of the curves, ΔE can be calculated. The values of ΔE of PP, *β*-PP, *β*-PP/T-talc (90 wt%/10 wt%), and *β*-PP/PP-*g*-MAH/T-talc (85 wt%/5 wt%/10 wt%) composite samples are 161.6, 173.6, 160.7, and 167.8 kJ/mol, respectively. It is clear that only the simultaneous addition of *β*-nucleator and T-talc into PP decreases ΔE slightly. From the kinetic viewpoint, the lower ΔE can be correlated with higher crystallization rate. It has been found the crystallization rate of *β*-PP/T-talc (90 wt%/10 wt%) composite is higher than those of the other samples, which has a good agreement with the change of ΔE. However, the addition of NT-C alone increases the ΔE and crystallization rate simultaneously. It had been reported that ΔE and crystallization rate increase at the same time with the addition of *β*-nucleating agents.[50,51] The crystallization process is controlled by two processes: nucleation and spherulitic growth. Zhao et al.[51] believed that nucleating agents might baffle the transfer of macromolecular segments from iPP melts to the crystal growth surface due to the weak interaction between nucleating agents and segments of iPP. The baffling effect might lead to the increase of ΔE, while nucleation was the controlling step during crystallization, the increase of nucleation rate leaded to the increase of the overall crystallization rate and crystallization temperature.

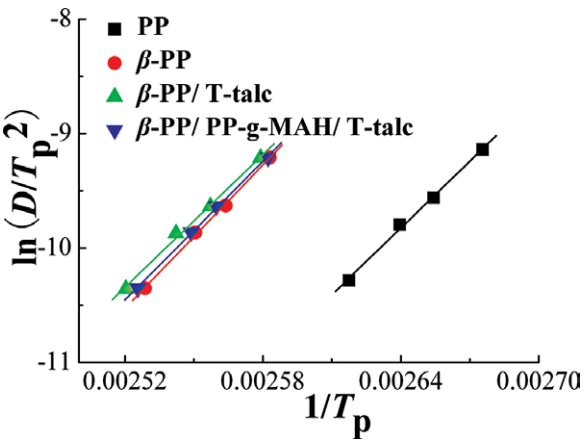

Figure 14. ln (D/T_p^2) versus $1/T_p$ for samples. [Color figure can be viewed in the online issue, which is available at wileyonlinelibrary.com.]

CONCLUSIONS

The crystallization, morphology and mechanical properties of *β*-PP/PP-*g*-MAH/ treated talc composites were investigated.

DSC results indicate that NT-C remarkably increase the content of *β*-phase but T-talc is an α-nucleating agent and suppresses the formation of *β*-modification, and PP-*g*-MAH is slightly unfavorable to the formation of *β*-form PP. T_c^{on} and T_c^{P} shift to higher temperatures after the addition of T-talc and NT-C, but the increments of these temperatures are limited as the increasing loading of T-talc. PP-*g*-MAH has a slight negative effect on the crystallization rate of PP.

WAXD results indicate T-talc restrains the formation of *β*-crystal and PP-*g*-MAH further decreases the amount of *β*-phase PP.

PLM observations show that addition of T-talc significantly decreases the amount of *β* spherulites but NT-C induces lots of colorful *β* spherulites. Both NT-C and T-talc greatly decreases the spherulitic size. The spherulitic morphology remains constant as the inclusion of PP-*g*-MAH with respect to *β*-PP/T-talc composites.

The results of SEM show that many microvoids are detected in the fractured surfaces of PP/T-talc and *β*-PP/T-talc composites, while the interface between PP and T-talc particles is blurry and the amount of microvoids visibly decreases after addition of PP-*g*-MAH.

The notched impact strength of *β*-PP/T-talc composites obtains the maximum value of 9.22 kJ m^{-2} at 2.5 wt% T-talc loading, which is higher than that of PP/T-talc composites, indicating the synergistic toughening effect of T-talc and *β*-phase. PP-*g*-MAH further increases the notched impact strength of *β*-PP/T-talc composites at low loading (≤2.5 wt% T-talc) because of better filler-matrix adhesion and compatibility.

The non-isothermal crystallization kinetics of *β*-PP/T-talc (90 wt%/10 wt%) and *β*-PP/PP-*g*-MAH/T-talc (85 wt%/5 wt%/10 wt%) composites can be well described by Jeziorny's and Mo's methods. The result shows that both NT-C and T-talc have a synergistic effect on accelerating the crystallization rate of PP

but PP-*g*-MAH has a slight negative effect on the crystallization rate of *β*-PP/T-talc composite. It is clear that simultaneous addition of NT-C and T-talc decreases the ΔE slightly but addition of NT-C alone increases the ΔE.

ACKNOWLEDGMENTS

This project was partially supported by A Project Funded by the Priority Academic Program Development of Jiangsu Higher Education Institutions (PAPD).

REFERENCES

1. Jahani, Y. *Polym. Adv. Technol.* **2011**, *22*, 942.
2. Gafur, M. A.; Nasrin R.; Mina M. F.; Bhuiyan M. A. H.; Tamba Y.; Asano T. *Polym. Degrad. Stab.* **2010**, *95*, 1818.
3. Meng, M. R.; Dou, Q. *J. Macromol. Sci. Phys.* **2009**, *48*, 213.
4. Dou, Q.; Meng, M.; Li, L. *Polym. Compos.* **2010**, *31*, 1572.
5. Maiti, S. N.; Sharma, K. K. *J. Mater. Sci.* **1992**, *27*, 4605.
6. Tjong, S. C.; Li, R. K. Y. *J. Vinyl Addit. Technol.* **1997**, *3*, 89.
7. de Medeiros, E. S.; Tocchetto, R. S.; de Carvalho, L. H.; Santos, I. M. G.; Souza, A. G. *J. Therm. Anal. Calorim.* **2001**, *66*, 523.
8. da Silva, A. L. N.; Rocha, M. C. G.; Moraes, M. A. R.; Valente, C. A. R.; Coutinho, F. M. B. *Polym. Test.* **2002**, *21*, 57.
9. Leong, Y. W.; Abu Bakar, M. B.; Mohd. Ishak, Z. A.; Ariffin, A. *J. Appl. Polym. Sci.* **2005**, *98*, 413.
10. Ai Wah, C.; Yub Choong, L.; Seng Neon, G. *Eur. Polym. J.* **2000**, *36*, 789.
11. Dou, Q.; Lu, Q. L.; Li H. D. *J. Elastomers Plast.* **2009**, *47*, 900.
12. Shi, Y. H.; Dou, Q. *Adv. Mater. Res.* **2011**, *233*, 2129.
13. Dou, Q. *J. Macromol. Sci. Phys.* **2007**, *46*, 1063.
14. Norton, D. R.; Keller, A. *Polymer* **1985**, *26*, 704.
15. Asanoa, T.; Imaizumia, K.; Tohyamaa, N.; Yoshidaa S. *J. Macromol. Sci. Phys.* **2005**, *43*, 639.
16. Varga, J.; Karger-Kocsis, J. *J. Polym. Sci. Part B: Polym. Phys.* **1996**, *34*, 657.
17. Torre, J.; Cortázar, M.; Gómez, M.; Ellis, G.; Marco, C. *J. Polym. Sci. Part B: Polym. Phys.* **2004**, *42*, 1949.
18. Zhang, Z.; Wang, C.; Yang, Z.; Chen, C.; Mai, K. *Polymer* **2008**, *49*, 5137.
19. Zhang, Z.; Tao, Y.; Yang, Z.; Mai, K. *Eur. Polym. J.* **2008**, *44*, 1955.
20. Zhang, Q. X.; Yu, Z. Z.; Xie, X. L.; Mai, Y. W. *Polymer* **2004**, *45*, 5985.
21. Meng M.; Dou, Q. *Mater. Sci. Eng. A* **2008**, *492*, 177.
22. Li, L.; Dou, Q. *J. Macromol. Sci. Phys.* **2011**, *50*, 831.
23. Li, L.; Dou, Q. *Polym. Compos.* **2010**, *31*, 966.
24. Han, L.; Li, X.; Li, Y.; Huang, T.; Wang, Y.; Wu, J.; Xiang, F. *Mater. Sci. Eng. A* **2010**, *527*, 3176.
25. Mai, J. H., Zhang, M. Q.; Rong, M. Z.; Barany, T.; Ruan, W. H. *Exp. Polym. Lett.* **2012**, *6*, 739.
26. Prachum, Y.; Adam Strauss, R. H.; Kiatkamjornwong, S. *J. Appl. Polym. Sci.* **2011**, *122*, 1066.
27. Zhang, N.; Zhang, Q.; Wang, K.; Deng, H.; Fu, Q. *J. Therm. Anal. Calorim.* **2012**, *107*, 733.
28. Lin, Z.; Zhang, Z.; Mai, K. *J. Appl. Polym. Sci.* **2012**, *125*, 61.
29. Varga, J.; Tóth, F. S. *Angew Makromol. Chem.* **1991**, *188*, 11.
30. Fujiyama, M. *Int. Polym. Proc.* **1998**, *13*, 411.
31. Shi, Y. H.; Dou, Q. *Polym. Plast. Tech. Eng.* **2012**, *51*, 1024.
32. Shi, Y. H.; Dou, Q. *J. Macromol. Sci. Phys.* DOI: 10.1080/00222348.2012.715873.
33. Shi, Y. H.; Dou, Q. *J. Therm. Anal. Calorim.* DOI: 10.1007/s10973-012-2611-0.
34. Varga, J. *J. Macromol. Sci. Phys.* **2002**, *41*, 1121.
35. Turner-Jones, A.; Aizlewood, J. M.; Beckett, D. R. *Makromol. Chem.* **1964**, *75*, 134.
36. Li, J. X.; Cheung, W. L. *Polymer* **1998**. *39*, 6935.
37. Varga, J. *J. Therm. Anal. Calorim.* **1999**, *56*, 1047.
38. Varga, J. *J. Therm. Anal.* **1986**, *31*, 165.
39. Tao, Y.; Pan, Y.; Zhang, Z.; Mai, K. *Eur. Polym. J.* **2008**, *44*, 1165.
40. Frihi, D.; Masenelli-Varlot, K.; Vigier, G.; Satha, H. *J. Appl. Polym. Sci.* **2009**, *114*, 3097.
41. Tjong, S. C.; Shen, J. S.; Li, R. K. Y. *Scripta Metal Mater.* **1995**, *33*, 503.
42. Tjong, S.C.; Shen, J. S.; Li, R. K. Y. *Polymer* **1996**, *37*, 2309.
43. Wang, Y., Shen, H.; Li, G.; Mai, K. *J. Appl. Polym. Sci.* **2009**, *113*, 1584.
44. Jeziorny, A. *Polymer* **1978**, *19*, 1142.
45. Liu, T. X.; Mo, Z. S.; Zhang, H. F. *J. Appl. Polym. Sci.* **1998**, *67*, 815.
46. Wunderlich, B. Macromolecular Physics, Vol.*2*: Crystal Nucleation, Growth, Annealing, Academic Press: New York, **1976**, Chapter VI.
47. Ding, Z.; Spruiell, J. E. *J. Polym. Sci. Part B : Polym. Phys.* **1997**, *35*, 1077.
48. Wang, J. B.; Dou, Q. *J. Macromol. Sci. Phys.* **2007**, *46*, 987.
49. Kissinger, H. *J. Res. Natl. Bur. Stand.* **1956**, *57*, 217.
50. Xu, L. L.; Zhang, X. J.; Xu, K.; Lin, S. Q.; Chen, M. C. *Polym. Int.* **2010**, *59*, 1441.
51. Zhao, S.; Cai, Z.; Xin, Z. *Polymer* **2008**, *49*, 2745.